Letter Vol. 6, No. 2 / February 2019 / Optica 135

optica

Probing near-field light–matter interactions with single-molecule lifetime imaging

D. Bouchet,[1] J. Scholler,[1] G. Blanquer,[1] Y. De Wilde,[1] I. Izeddin,[1,2] and V. Krachmalnicoff[1,3]

[1]Institut Langevin, ESPCI Paris, CNRS, PSL University, 1 rue Jussieu, Paris 75005, France
[2]e-mail: ignacio.izeddin@espci.fr
[3]e-mail: valentina.krachmalnicoff@espci.fr

Received 15 November 2018; revised 30 December 2018; accepted 2 January 2019 (Doc. ID 352110); published 25 January 2019

Nanophotonics offers a promising range of applications spanning from the development of efficient solar cells to quantum communications and biosensing. However, the ability to efficiently couple fluorescent emitters with nanostructured materials requires one to probe light–matter interactions at a subwavelength resolution, which remains experimentally challenging. Here, we introduce an approach to perform super-resolved fluorescence lifetime measurements on samples that are densely labeled with photo-activatable fluorescent molecules. The simultaneous measurement of the position and the decay rate of the molecules provides direct access to the local density of states (LDOS) at the nanoscale. We experimentally demonstrate the performance of the technique by studying the LDOS variations induced in the near field of a silver nanowire, and we show via a Cramér–Rao analysis that the proposed experimental setup enables a single-molecule localization precision of 6 nm.

https://doi.org/10.1364/OPTICA.6.000135

Single fluorescent emitters constitute excellent probes to access the evanescent near field of a nanostructure with far-field measurements. Indeed, the advent of super-resolution microscopy in the field of biophotonics has uncapped an unprecedented detail of observation of subcellular structures, revealing structural features of tens of nanometers [1–3], 1 order of magnitude below the resolution limit imposed by the diffraction of light. While the main super-resolution approaches are based on fluorescence intensity measurements, there exists a strong interest in developing techniques capable of probing lifetime variations at the nanoscale by associating fluorescence lifetime imaging microscopy (FLIM) with subwavelength spatial information. The far-reaching potential of fluorescence lifetime imaging with nanometer resolution is straightforward not only for biological studies [4,5] but also for nanophotonics applications [6,7], as the lifetime of fluorescent emitters is inversely proportional to the local density of states (LDOS) [8].

In the last few years, different experimental approaches have been proposed to achieve lifetime measurements at the nanoscale. Super-resolution lifetime imaging was first demonstrated in combination with stimulated emission-depletion (STED) microscopy [9], mostly used for biological applications, and more recently by making use of scanning-probe microscopy to characterize the response of nanostructured plasmonic [10–14] or dielectric [15] materials to light. Despite the contribution of these methods to nanoscale imaging, a wide-field scheme, rather than a scanning approach, is essential in order to study dynamic phenomena and to reach molecular resolution. Several groups have recently proposed wide-field approaches to obtain super-resolved LDOS measurements. The association of wide-field localization with a scanning scheme was used to probe lifetime variations induced by periodic structures [16]. Elegant techniques (although arduous to master) were implemented to measure the lifetime of single quantum dots positioned with microfluidic flow control [17,18] or using surface-bound motor proteins [19], allowing one to image LDOS variations induced by plasmonic nanostructures. Other methods based on point accumulation for imaging in nanoscale topography (PAINT) [20,21] and photo-activated localization microscopy (PALM) [22] need numerical simulations to estimate the LDOS from intensity-based measurements.

In this Letter, we introduce a novel approach that overpasses these limitations and combines lifetime and super-resolved spatial information based on stochastic optical reconstruction microscopy (STORM) [3], a stochastic imaging technique widely used in biological imaging [23]. This method allows us to map the lifetime τ of stochastically photo-activated single molecules in close vicinity of a densely labeled nanostructure. It can be readily implemented with a standard microscope and can be applied to biological samples or artificially fabricated nanostructures, either dielectric, metallic, or hybrid metallo/dielectric. Here, we demonstrate the performance of the technique by mapping the LDOS variations induced by a silver nanowire on single molecules located a few nanometers apart. Plasmonic nanowires are an ideal playground to demonstrate the ability of a super-resolved technique to measure light–matter interactions on the nanometer range. They induce strong variations of the lifetime of nearby emitters on the nanometer scale, highlighting the large dynamic range in terms of lifetime modification explorable with our technique. Moreover, due to their geometric simplicity, they enable handleable theoretical studies easily comparable to experimental results.

The sample consists of silver nanowires on a glass coverslip, wholly covered with photo-activatable fluorescent molecules, and is illuminated in a wide field with a pulsed laser through an oil immersion objective mounted on an inverted microscope. The studied nanowires have a diameter of ∼115 nm and a length of several tens of micronmeters. Their large longitudinal dimension ensures that they weakly radiate to the far field, and therefore strongly limits the shift in the apparent position of the emitters that has been observed for resonant nanostructures [18,20,24]. The specificity of our method relies on the simultaneous detection of fluorescence photons, through the same microscope objective as the one used for the excitation, on an electron-multiplying charge-coupled device (EM-CCD) camera for super-localization and on a single-photon avalanche diode (SPAD) coupled to a time-correlated single-photon counting (TCSPC) system for lifetime measurements (see Section 1 of Supplement 1). The EM-CCD camera records wide-field images of the sample with a field of view of tens of micrometers on the sample plane. In contrast, the SPAD, which is a single-channel detector, is conjugated with the center of the camera image via a 50 μm confocal pinhole and covers an area on the sample plane of ∼1 μm^2. By setting the excitation and photo-activation laser power so that no more than one molecule is active at a given time on the area conjugated to the SPAD, the decay rate $\Gamma = 1/\tau$ can be properly estimated for each individual molecule and can be associated to its position.

This approach is illustrated in Fig. 1. A single fluorescent molecule is identified on a sequence of wide-field images [Fig. 1(a)], and the position of this molecule is estimated by fitting a two-dimensional Gaussian function to the measured point spread function [Fig. 1(b)]. At the same time, the detection of a fluorescent molecule appears as a burst on the signal of the SPAD time trace [Fig. 1(c)]. For each SPAD burst, we build the associated decay histogram with a time resolution of 16 ps [Figs. 1(d) and 1(e)]. To estimate the decay rate, the convolution of the instrument response function (IRF) and a decreasing mono-exponential function is fitted to the decay histogram. Based on the time correlation between the events detected by the camera and the SPAD (see Section 2 of Supplement 1), we can associate position and decay rate for a large number of photo-activated molecules detected in a single experiment and obtain the super-resolved decay rate map shown in Fig. 1(f). This map is reconstructed from simultaneous position and decay rate measurements of 3119 molecules located in a sample region of 1 μm^2 containing one silver nanowire. The typical localization precision, calculated via a Cramér–Rao lower bound analysis as explained below, is of the order of 6 nm. Spatial variations of the decay rate are observed well below the diffraction limit, demonstrating the ability of the technique to obtain super-resolved LDOS images in a wide-field optical configuration.

A unique insight as allowed by this new approach is revealed by the study of the density of detected molecules along the center of the nanowire axis (see Section 3 of Supplement 1). Figure 2(a) shows that, on average, twice as many molecules are detected for a distance to the nanowire axis $d = \pm 50$ nm than for $d = 0$ nm. Indeed, the interaction between the excitation field and the nanowire results in a non-uniform excitation intensity distribution, as shown in Fig. 2(b) by finite difference time-domain (FDTD) simulations (see Section 4 of Supplement 1). A local enhancement of the excitation intensity is observed on the sides of the nanowire, with a lateral extension of about

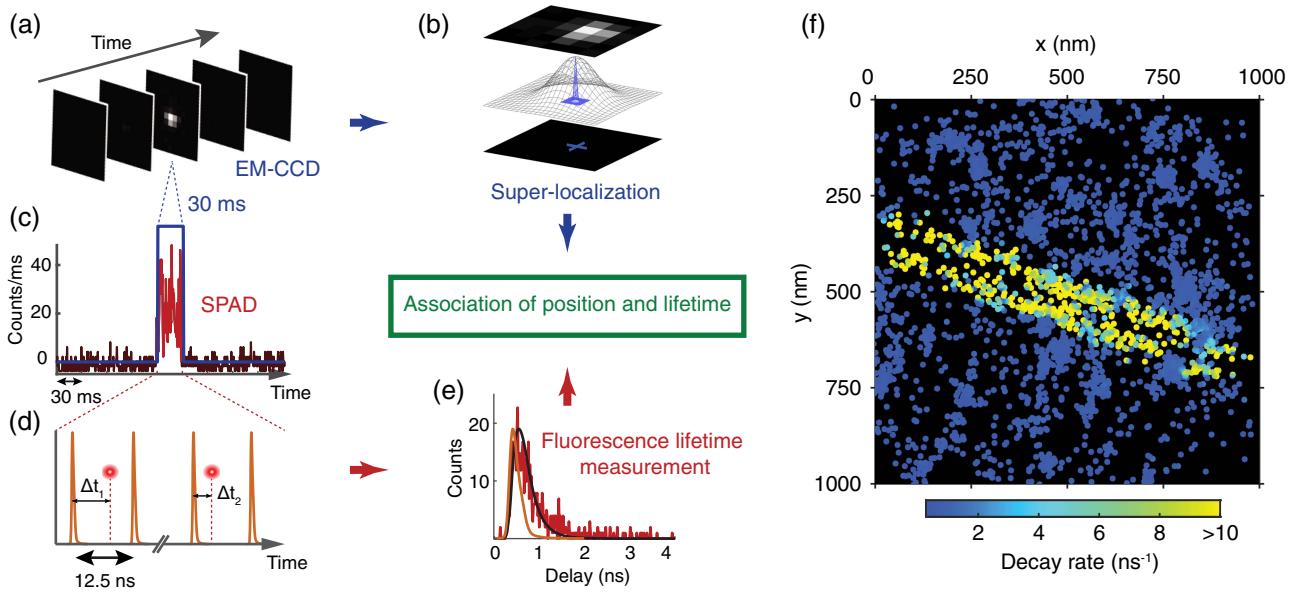

Fig. 1. Super-resolved LDOS mapping of a silver nanowire. (a) The EM-CCD camera acquires 31 frames per second, with an exposure time of 30 ms per frame and a field of view of tens of micrometers. A single fluorescent molecule is detected on the third frame of the sequence shown here. An image cropped around the molecule is shown here for the sake of simplicity. (b) The position of the molecule is estimated by fitting a two-dimensional Gaussian function to the measured point spread function (PSF). The PSF covers an area of ∼9 pixels (pixel size = 160 nm). (c) At the same time, the SPAD detects a fluorescence burst from this molecule. (d) Short laser pulses were used to excite this molecule. For each photon detected during the fluorescence burst, the time difference between excitation and emission can be determined with picosecond precision. (e) These photons are used to construct a decay histogram. The convolution of the IRF and a decreasing mono-exponential function is then fitted to this histogram in order to estimate the fluorescence decay rate of the molecule. The IRF is shown in orange. (f) Reconstructed decay rate map. Each dot represents the position of a detected molecule, and its diameter is fixed at 15 nm, which is the typical full width at half-maximum (FWHM) of the probability density function followed by the position estimates. If several molecules are detected within the same area, we show their average decay rate on the map.

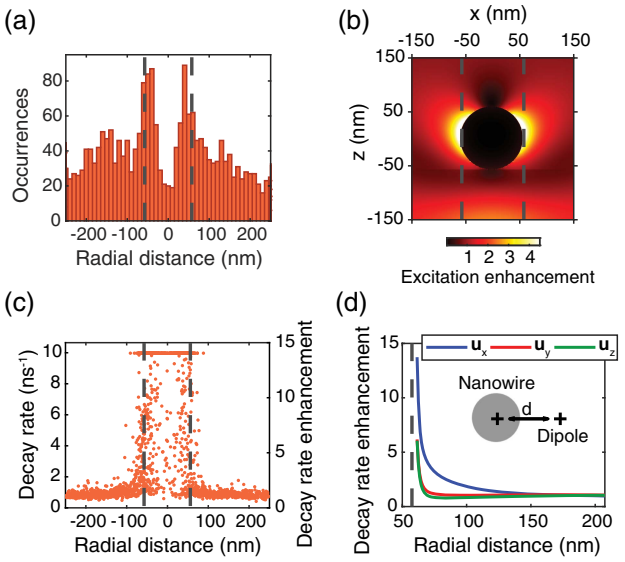

Fig. 2. (a) Number of detected molecules as a function of the distance to the nanowire axis. (b) Time-averaged intensity of the excitation field in the vicinity of the silver nanowire calculated from the results of a FDTD simulation. On these figures, dashed lines represent the estimated position of the nanowire edges. (c) Distribution of decay rate versus distance to the wire axis. The highest decay rate that can be measured, limited by the IRF of the setup, is 10 ns^{-1}. (d) Decay rate enhancement as a function of the distance to the nanowire for the three orientations of the dipole moment. The inset shows a cross section of the system numerically studied.

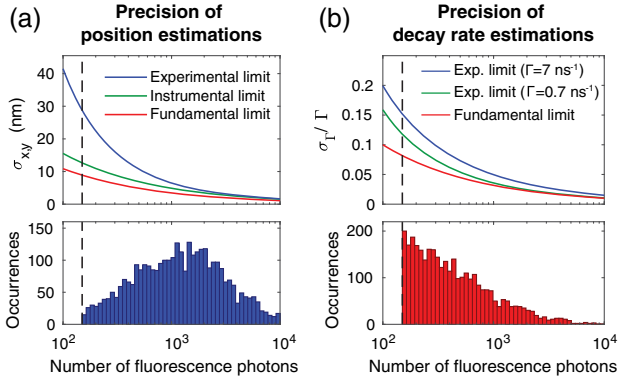

Fig. 3. (a) Top, Cramér–Rao bound on the standard error on the position estimates as a function of the number of fluorescence photons detected by the camera. Bottom, distribution of the number of fluorescence photons detected by the camera from the single molecules. (b) Top, Cramér–Rao bound on the standard error on the decay rate estimates as a function of the number of fluorescence photons detected by the SPAD. Bottom, distribution of the number of fluorescence photons detected by the SPAD from the single molecules. On these figures, dashed lines represent the threshold condition $N > 150$ used for data analysis.

20 nm, as well as an extinction of the excitation intensity on the top of the wire. Therefore, the molecules located in the higher excitation intensity regions have a larger probability to be detected, supporting the observed variations of the density of detected molecules. Furthermore, the image is formed by a two-dimensional projection of fluorescent events around a cylindrical nano-object. This also affects the apparent density of detected molecules.

In order to get a deeper insight into the observed decay rate variations, we further studied the dependence of the decay rate on the distance d to the nanowire axis [Fig. 2(c)]. Molecules detected far from the nanowire axis ($d > 200$ nm) show an average value of the decay rate of 0.68 ns^{-1} with a standard deviation of 0.17 ns^{-1}. In contrast, the decay rate is higher than 10 ns^{-1} for many molecules detected at distances $d < 60$ nm from the nanowire axis. This leads to a decay rate enhancement of a factor 15, only limited by the IRF of the setup (see Section 5 of Supplement 1). This measurement confirms that molecules with the largest decay rates are those attached to the nanowire or in its closest vicinity. We further numerically simulated the enhancement of the decay rate induced by the presence of the nanowire for three orthogonal dipole moment orientations [Fig. 2(d)]. Experimental and numerical results are in good qualitative agreement, supporting the validity of the experimental technique. Different dipole moment orientations can explain the lifetime dispersion observed in the vicinity of the nanowire.

The performance of the proposed method ultimately relies on the precision at which we can estimate both the position and the decay rate of the detected single fluorophores. We can assess a lower bound on these parameters by calculating the Cramér–Rao lower bound [25] on the standard error of the position and lifetime estimators, respectively noted $\sigma_{x,y}$ and σ_Γ (see Sections 6 and 7 of Supplement 1). Such analysis is standard in localization microscopy to assess the localization precision [26,27]. Figure 3(a) shows the dependence of $\sigma_{x,y}$ upon the number of fluorescence photons detected by the EM-CCD camera. The fundamental limit (red curve) is set by the shot noise and the finite pixel size as sources of error on the measurement. The instrumental limit (green curve) also accounts for the readout noise of the camera and the noise introduced by the electron multiplying process. The actual limit of our experiment (blue curve) is calculated by considering additional sources of noise such as substrate luminescence. The number of fluorescence photons experimentally detected by the camera from each molecule ranges from 150 to more than 10^4 fluorescence photons with a median value of 1228 photons [Fig. 3(a), bottom]. With this value, the Cramér–Rao bound for position estimations is 6 nm.

A similar analysis can also be performed for lifetime estimations [28,29]. The fundamental limit on the relative standard error of decay rate estimators σ_Γ/Γ is simply given by $1/\sqrt{N}$, where N is the number of detected photons [Fig. 3(b), red curve]. We calculated the Cramér–Rao bound for $\Gamma = 0.7$ ns^{-1} (molecules on glass) and $\Gamma = 7$ ns^{-1} (molecules close to the nanowire), which corresponds to a lifetime of 140 ps, comparable to the FWHM of the IRF (240 ps). As expected, σ_Γ/Γ deviates from the fundamental limit when the number of measured fluorescence photons is smaller than 1000 due to the influence of background noise. In the experiment, the median value of detected photons is 367 photons [Fig. 3(b), bottom]. For this value, σ_Γ/Γ ranges from 8% to 10% depending on the value of Γ.

The Cramér–Rao analysis thus demonstrates that the proposed experimental setup enables state-of-the-art measurements of light–matter interactions with a localization precision of 6 nm together with a relative error of 10% for lifetime estimations. Future prospects will include accessing the axial position of

the detected molecules with the implementation of three-dimensional localization methods [30–33]. The technique can notably be adapted to perform three-dimensional imaging using metal-induced energy transfer, as suggested by a recent article reporting three-dimensional localization for sparsely distributed single molecules [34]. Additionally, by taking advantage of SPAD arrays constituted of several independent channels [35], a field of view of tens of micrometers in the sample plane could be reached, opening a wide range of interesting opportunities for imaging and sensing applications. The acquisition time could also be reduced by actively optimizing the number of molecules simultaneously photo-activated on the region conjugated to the SPAD. Multiple simultaneous detections could be treated with an improved detection, fitting, and reconstruction algorithm.

The readiness of the technique to be implemented with a standard microscope suggests a great potential to rapidly expand into a wide variety of applications ranging from nanophotonics and plasmonics to biophotonics. Topical applications in nanophotonics include the direct characterization of samples presenting rich LDOS patterns and strongly confined electromagnetic fields, with concrete perspectives for the study of light localization in strongly scattering media [36,37]. The technique is not constrained to the fluorophores used in the present realization, but can be extended to photo-activatable fluorophores of different wavelengths and to DNA-PAINT for an *a priori* knowledge of the fluorophore position. Thanks to these extensions, it will be possible to characterize the resonant and non-resonant behavior of a nanostructure and to tackle the mislocalization of resonant fluorophores with fluorescence lifetime measurements. In the field of biophotonics, wide-field FLIM images with nanometer resolution will allow us to probe local dynamic phenomena in living cells. We also foresee that, by associating our approach with techniques based on Förster resonance energy transfer (FRET), *in cellulo* nanoscale imaging of molecule–molecule interactions will soon become within reach.

Funding. Ville de Paris (Emergences 2015); Agence Nationale de la Recherche (ANR) (ANR-10_LABX-24, ANR-10- IDEX-0001-02 PSL*, ANR-17-CE09-0006).

Acknowledgment. The authors thank S. Bidault for helping in sample preparation, A. C. Boccara for sharing his insights about the manuscript, and I. Rech, A. Gulinatti, and A. Giudice for providing the PMD-R detector.

See Supplement 1 for supporting content.

REFERENCES

1. E. Betzig, G. H. Patterson, R. Sougrat, O. W. Lindwasser, S. Olenych, J. S. Bonifacino, M. W. Davidson, J. Lippincott-Schwartz, and H. F. Hess, Science **313**, 1642 (2006).
2. S. T. Hess, T. P. K. Girirajan, and M. D. Mason, Biophys. J. **91**, 4258 (2006).
3. M. J. Rust, M. Bates, and X. Zhuang, Nat. Methods **3**, 793 (2006).
4. M. Y. Berezin and S. Achilefu, Chem. Rev. **110**, 2641 (2010).
5. W. Becker, J. Microsc. **247**, 119 (2012).
6. A. F. Koenderink, A. Alù, and A. Polman, Science **348**, 516 (2015).
7. E. D. Fabrizio, S. Schlücker, J. Wenger, R. Regmi, H. Rigneault, G. Calafiore, M. West, S. Cabrini, M. Fleischer, N. F. V. Hulst, M. F. Garcia-Parajo, A. Pucci, D. Cojoc, C. A. E. Hauser, and M. Ni, J. Opt. **18**, 063003 (2016).
8. R. Carminati, A. Cazé, D. Cao, F. Peragut, V. Krachmalnicoff, R. Pierrat, and Y. De Wilde, Surf. Sci. Rep. **70**, 1 (2015).
9. E. Auksorius, B. R. Boruah, C. Dunsby, P. M. P. Lanigan, G. Kennedy, M. A. A. Neil, and P. M. W. French, Opt. Lett. **33**, 113 (2008).
10. M. Frimmer, Y. Chen, and A. Koenderink, Phys. Rev. Lett. **107**, 123602 (2011).
11. V. Krachmalnicoff, D. Cao, A. Cazé, E. Castanié, R. Pierrat, N. Bardou, S. Collin, R. Carminati, and Y. De Wilde, Opt. Express **21**, 11536 (2013).
12. R. Beams, D. Smith, T. W. Johnson, S.-H. Oh, L. Novotny, and A. N. Vamivakas, Nano Lett. **13**, 3807 (2013).
13. A. W. Schell, P. Engel, J. F. M. Werra, C. Wolff, K. Busch, and O. Benson, Nano Lett. **14**, 2623 (2014).
14. A. Singh, G. Calbris, and N. F. van Hulst, Nano Lett. **14**, 4715 (2014).
15. D. Bouchet, M. Mivelle, J. Proust, B. Gallas, I. Ozerov, M. F. Garcia-Parajo, A. Gulinatti, I. Rech, Y. De Wilde, N. Bonod, V. Krachmalnicoff, and S. Bidault, Phys. Rev. Appl. **6**, 064016 (2016).
16. K. Guo, M. A. Verschuuren, and A. F. Koenderink, Optica **3**, 289 (2016).
17. C. Ropp, Z. Cummins, S. Nah, J. T. Fourkas, B. Shapiro, and E. Waks, Nat. Commun. **4**, 1447 (2013).
18. C. Ropp, Z. Cummins, S. Nah, J. T. Fourkas, B. Shapiro, and E. Waks, Nat. Commun. **6**, 6558 (2015).
19. H. Groß, H. S. Heil, J. Ehrig, F. W. Schwarz, B. Hecht, and S. Diez, Nat. Nanotechnol. **13**, 691 (2018).
20. E. Wertz, B. P. Isaacoff, J. D. Flynn, and J. S. Biteen, Nano Lett. **15**, 2662 (2015).
21. D. L. Mack, E. Cortés, V. Giannini, P. Török, T. Roschuk, and S. A. Maier, Nat. Commun. **8**, 14513 (2017).
22. E. Johlin, J. Solari, S. A. Mann, J. Wang, T. S. Shimizu, and E. C. Garnett, Nat. Commun. **7**, 13950 (2016).
23. B. Huang, H. Babcock, and X. Zhuang, Cell **143**, 1047 (2010).
24. M. Raab, C. Vietz, F. D. Stefani, G. P. Acuna, and P. Tinnefeld, Nat. Commun. **8**, 13966 (2017).
25. S. Kay, *Fundamentals of Statistical Processing Vol. I: Estimation Theory* (Prentice Hall, 1993).
26. H. Deschout, F. C. Zanacchi, M. Mlodzianoski, A. Diaspro, J. Bewersdorf, S. T. Hess, and K. Braeckmans, Nat. Methods **11**, 253 (2014).
27. J. Chao, E. S. Ward, and R. J. Ober, J. Opt. Soc. Am. A **33**, B36 (2016).
28. M. Köllner and J. Wolfrum, Chem. Phys. Lett. **200**, 199 (1992).
29. D. Bouchet, V. Krachmalnicoff, and I. Izeddin, "Fisher information theory for optimised lifetime estimations in time-resolved fluorescence microscopy," arXiv:1809.04149 (2018).
30. B. Hajj, M. E. Beheiry, I. Izeddin, X. Darzacq, and M. Dahan, Phys. Chem. Chem. Phys. **16**, 16340 (2014).
31. A. I. Chizhik, J. Rother, I. Gregor, A. Janshoff, and J. Enderlein, Nat. Photonics **8**, 124 (2014).
32. N. Bourg, C. Mayet, G. Dupuis, T. Barroca, P. Bon, S. Lécart, E. Fort, and S. Lévéque-Fort, Nat. Photonics **9**, 587 (2015).
33. S. Isbaner, N. Karedla, I. Kaminska, D. Ruhlandt, M. Raab, J. Bohlen, A. Chizhik, I. Gregor, P. Tinnefeld, J. Enderlein, and R. Tsukanov, Nano Lett. **18**, 2616 (2018).
34. N. Karedla, A. M. Chizhik, S. C. Stein, D. Ruhlandt, I. Gregor, A. I. Chizhik, and J. Enderlein, J. Chem. Phys. **148**, 204201 (2018).
35. A. Cuccato, S. Antonioli, M. Crotti, I. Labanca, A. Gulinatti, I. Rech, and M. Ghioni, IEEE Photon. J. **5**, 6801514 (2013).
36. R. Sapienza, P. Bondareff, R. Pierrat, B. Habert, R. Carminati, and N. F. van Hulst, Phys. Rev. Lett. **106**, 163902 (2011).
37. F. Riboli, N. Caselli, S. Vignolini, F. Intonti, K. Vynck, P. Barthelemy, A. Gerardino, L. Balet, L. H. Li, A. Fiore, M. Gurioli, and D. S. Wiersma, Nat. Mater. **13**, 720 (2014).